

Electronic Supplementary Information

Improvement of the Electron Collection Efficiency in Porous Hematite Using a Thin Iron Oxide Underlayer: Towards Efficient All-Iron Based Photoelectrodes.

Nicola Dalle Carbonare,^a Stefano Carli,^a Roberto Argazzi,^b Michele Orlandi,^c Nicola Bazzanella,^c Antonio Miotello,^c Stefano Caramori,^{,a} Carlo A. Bignozzi^{*,a}*

^a Department of Chemical and Pharmaceutical Sciences, University of Ferrara, via Fossato di Mortara 17-27, 44121 Ferrara, Italy

^b CNR/ISOF c/o Department of Chemical and Pharmaceutical Sciences, University of Ferrara, via Fossato di Mortara 17-27, 44121 Ferrara, Italy

^c Department of Physics, University of Trento, via Sommarive 14, I-38123 Povo, Trento, Italy

Table of contents

		Page
Figure S1	Top-view images of HTL-1-4 samples	S3
Table S1	Reproducibility of the thickness measurement with cross-section SEM analysis of HTL samples	S3
Figure S2	XRD of iron oxide powders at different annealing treatment	S4
Figure S3	Cross-sectional SEM image of MPH deposited on HTL-3 and annealed at 800°C	S4
Figure S4	Top-view SEM images of MPH deposited over FTO and annealed at 550 °C and 800 °C	S5
Figure S5	EDS analysis of MPH sample before and after 800°C annealing	S6
Figure S6	Micro-Raman spectra of HTL-1-4 samples and bare FTO	S7
Figure S7	XRD of MPH and HTL-3-MPH samples after 800°C annealing	S8
Figure S8	Background subtracted absorbance (390 nm) versus the number of spin coating runs (1-4) adopted to obtain HTL-1-4 samples	S8
Figure S9	Cross sectional view of MPH deposited on FTO and annealed at 800 °C	S9
Figure S10	Chronoamperometry of MPH, HTL-3-MPH and HTL-3-MPH+Fe-OEC	S9
Figure S11	Average <i>J-V</i> response of MPH, HTL-3-MPH and HTL-3-MPH+Fe-OEC	S10
Figure S12	<i>JV</i> curves of HTL-3 sample functionalized with Fe-OEC.	S10
Figure S13	IPCE spectra of HTL-3-MPH and the sum of the separated response of the two layers	S11
Figure S14	Photovoltage decays of MPH, HTL-3 and HTL-3-MPH samples recorded in a KOH solution of $K_4[Fe(CN)_6]/K_3[Fe(CN)_6]$ at different concentration	S12
Figure S15	Nyquist plot (0 V vs SCE) of MPH, HTL-3 and HTL-3-MPH with and without Fe-OEC	S13
Figure S16	Derivative of the <i>J-V</i> curve compared to R_{tot}^{-1} for HTL-3, MPH, HTL-3-MPH and HTL-3-MPH with Fe-OEC samples	S14
Figure S17	Mixed plot of <i>J-V</i> curve, R_3 and CPE2 values obtained for HTL-3, MPH, HTL-3-MPH and HTL-3-MPH with Fe-OEC under AM 1.5G illumination	S15
Figure S18	Mott-Schottky plot of MPH, HTL-3 and HTL-3-MPH samples	S16
Figure S19	Photoluminescence spectra of MPH and HTL-3-MPH.	S17

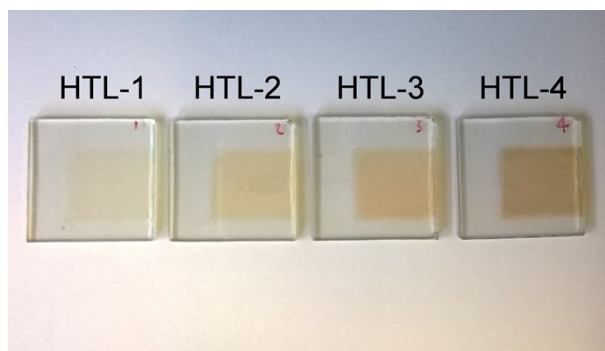


Figure S1. Top-view images of HTL-1-4 samples.

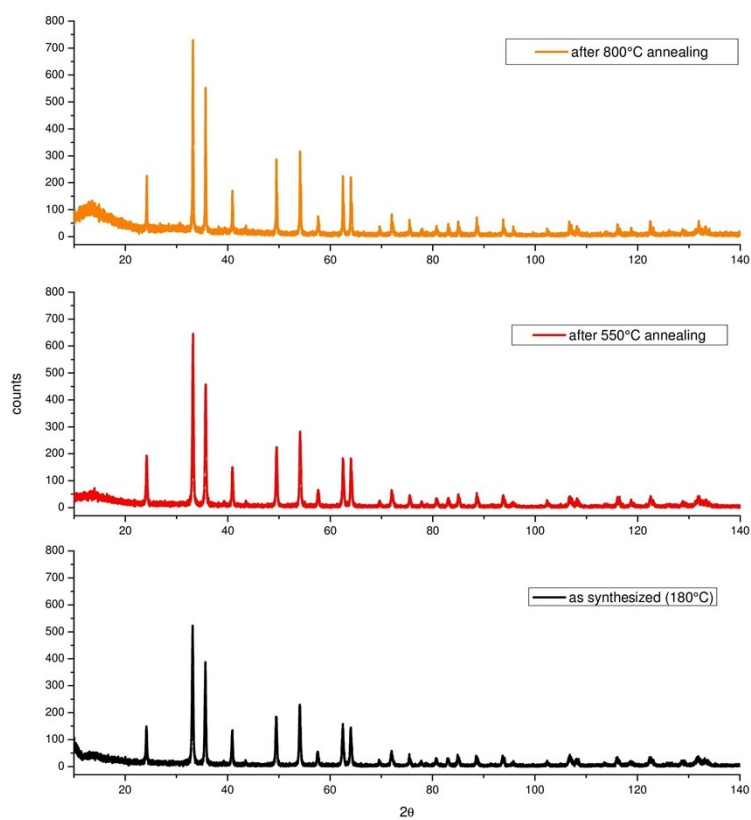


Figure S2. XRD of iron oxide powder as synthesized in autoclave at 180°C for 12 hours (black trace), after annealing at 550°C for 2 hours (red traces) and after 800°C treatment for 10 minutes (orange trace).

Sample	Number of measurements	Average Thickness	Standard Deviation
1	22	14	1.2
2	11	19	1.1
3	18	32	6.2
4	17	40	7.1

Table S1. Analysis of the reproducibility of the thickness of HTL samples measurement with the cross-section SEM analysis. Measurements were taken at a minimum of 3 and a maximum of 5 different locations along the film section. Outliers have not been discarded when calculating Standard Deviation.

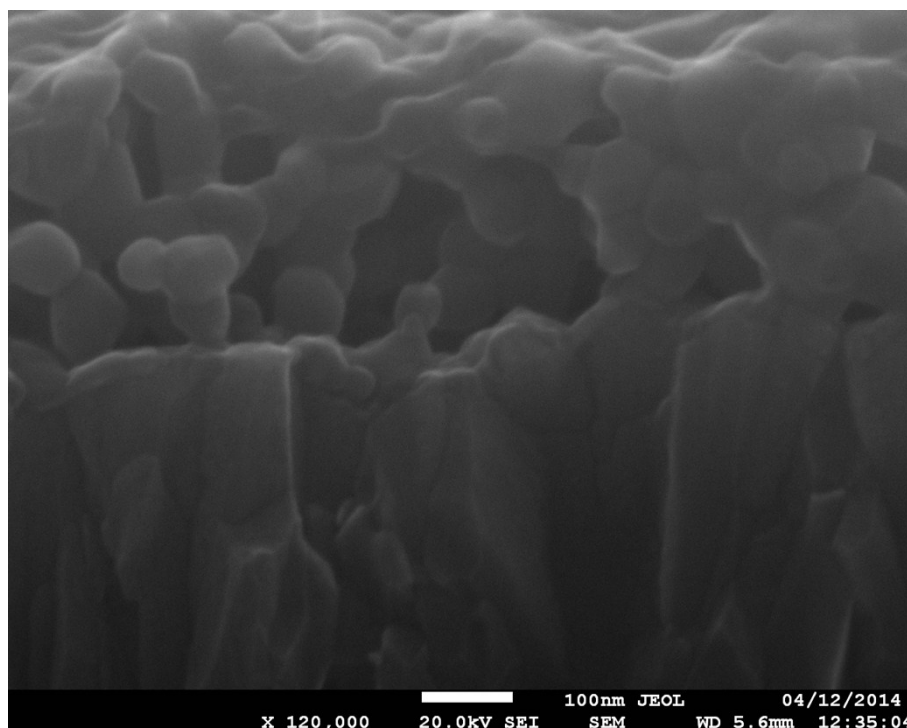


Figure S3 Cross-sectional SEM image of MPH deposited on HTL-3 and annealed at 800°C.

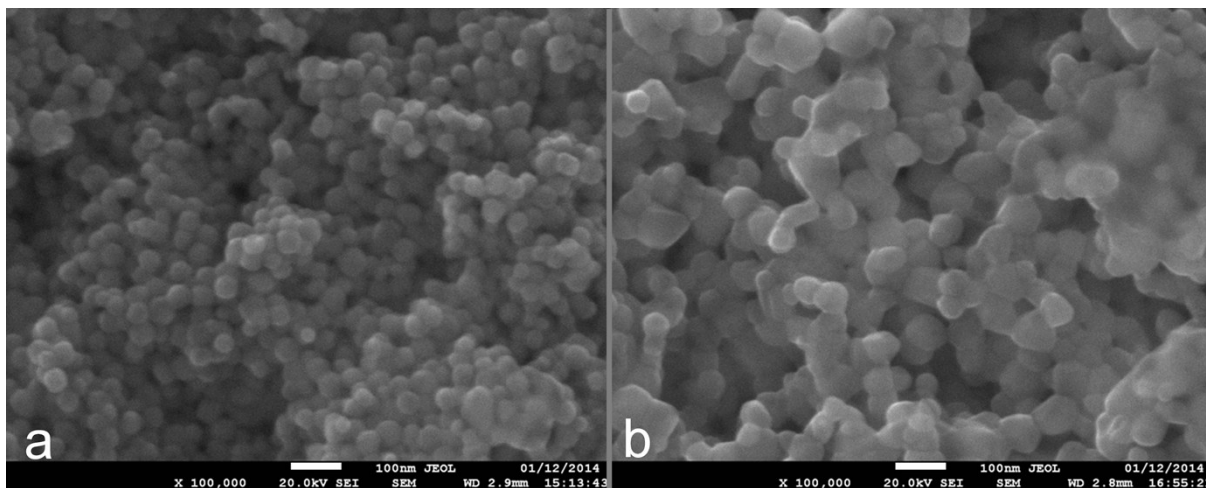


Figure S4 Top-view SEM images of MPH electrophoretically deposited over FTO and annealed at (a) 550 °C and (b) 800 °C.

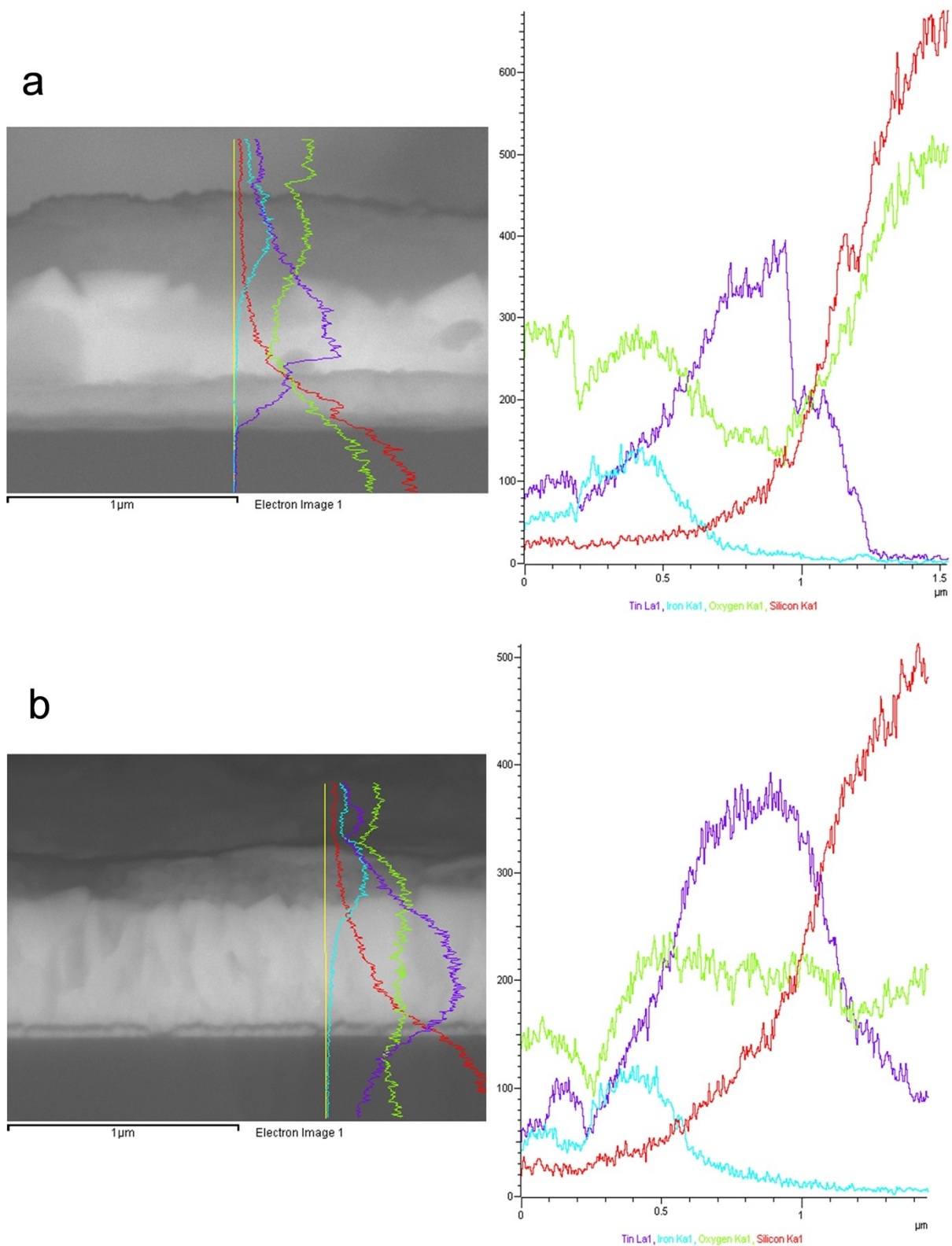


Figure S5 Cross sectional energy dispersive analysis (EDS) of MPH sample (a) before and (b) after 800°C annealing. The FTO/glass interface can be identified between 0.9 and 1.1 μm and

the hematite/FTO interface between 0.5 and 0.7 μm . The interface air/hematite, the actual surface, lies at about 0.1-0.2 μm .

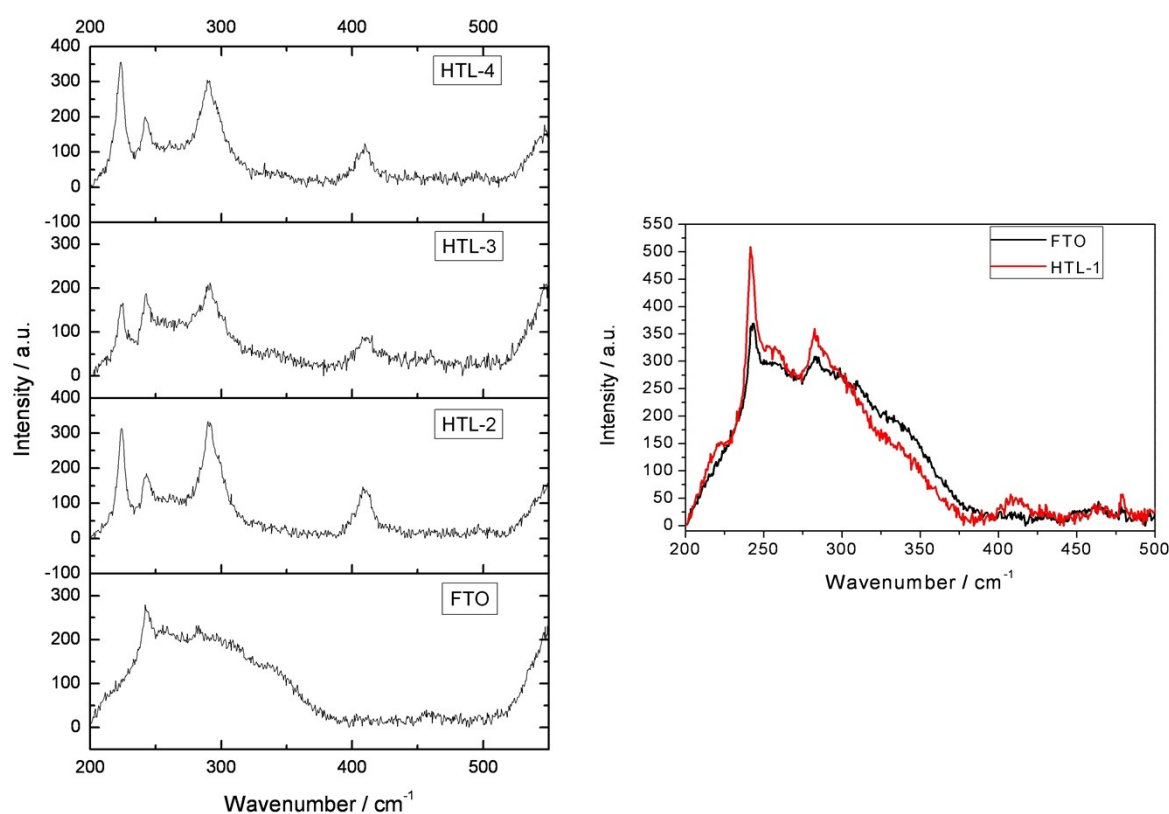


Figure S6 (left) Micro-Raman spectra of HTL-2-4 samples and bare FTO (shown for reference). (right) Micro-Raman spectra of HTL-1 (red line) and bare FTO (black line). While for MPH samples (Figure 4) the film is thick enough (> 300 nm in all samples) that the FTO contribute to the overall Raman signal is negligible, the spectra for HTL-1-4 show a convolution of the hematite signal with the underlying FTO signal. This is evident in particular for HTL-1 (right), where a clear identification of hematite on the surface is not possible. The diagnostic peaks for the presence of hematite can instead be revealed for HTL-2-4 (left).

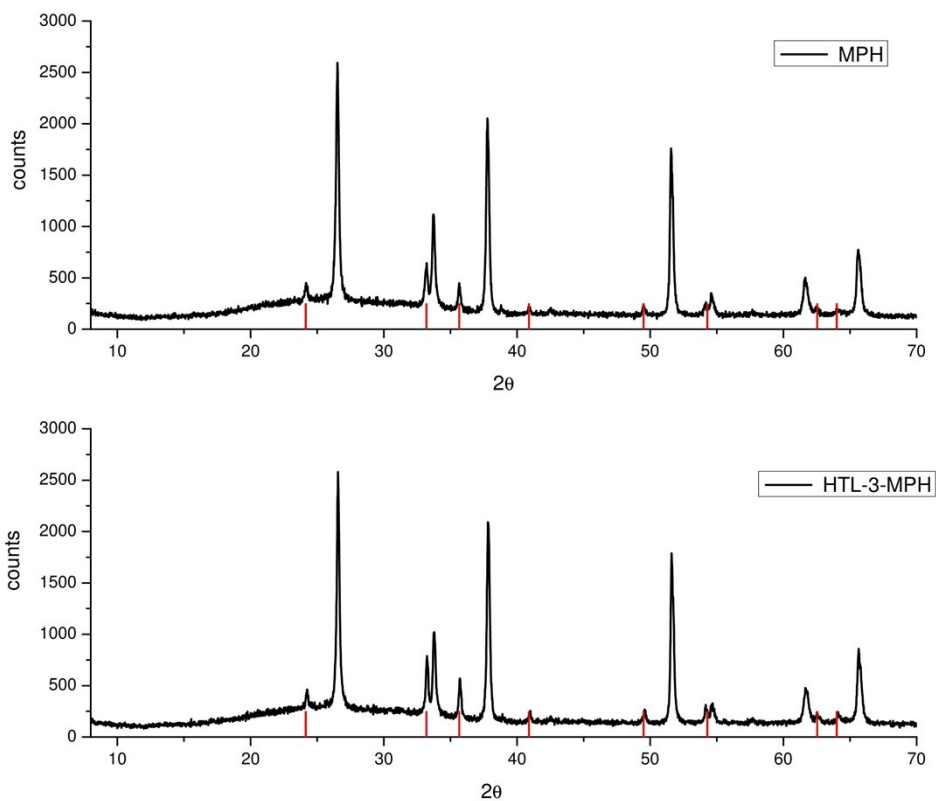


Figure S7 XRD of MPH and HTL-3-MPH samples after 800°C annealing. Red bars in the diffractograms indicate α -Fe₂O₃ signals.

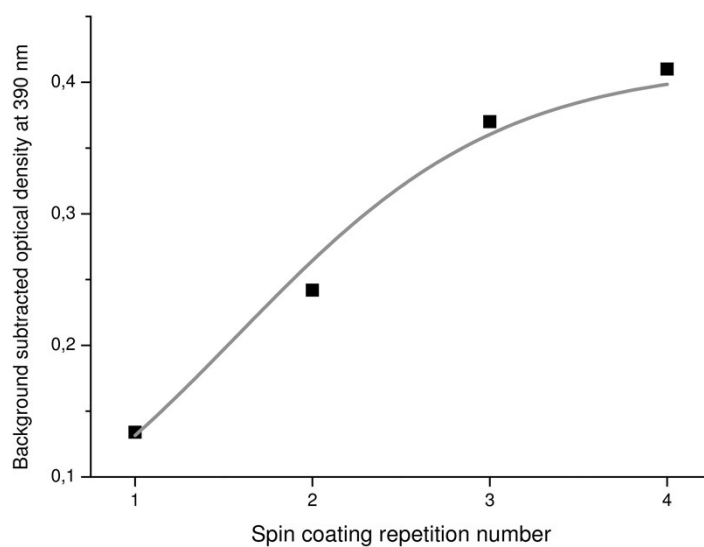


Figure S8 Plot of the background subtracted absorbance measured at 390 nm versus the number of spin coating runs (1-4) adopted to obtain HTL-1-4 samples.

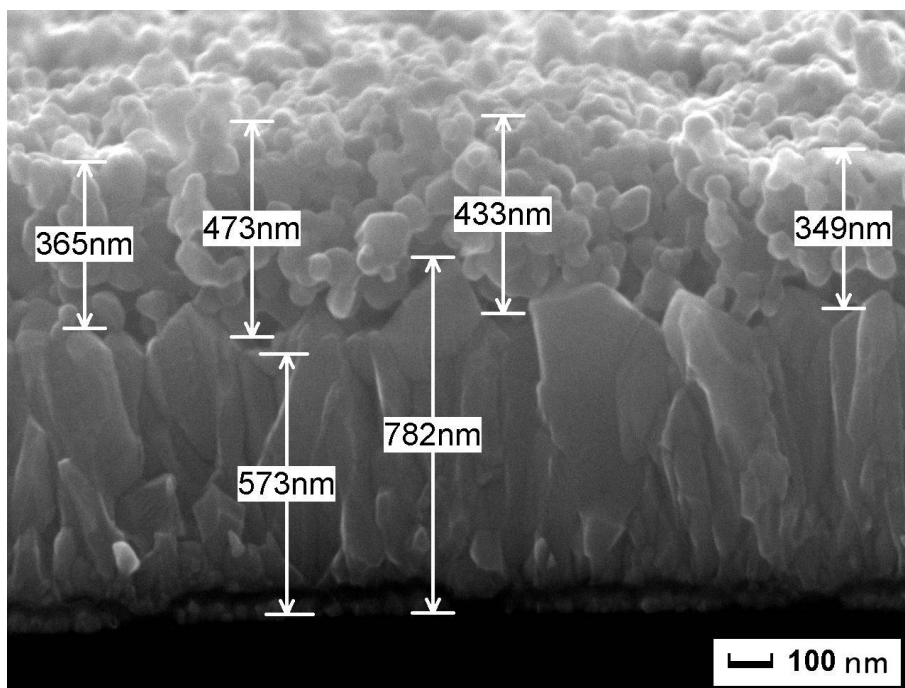


Figure S9 Cross sectional view of MPH electrophoretically deposited on bare FTO and annealed at 800 °C.

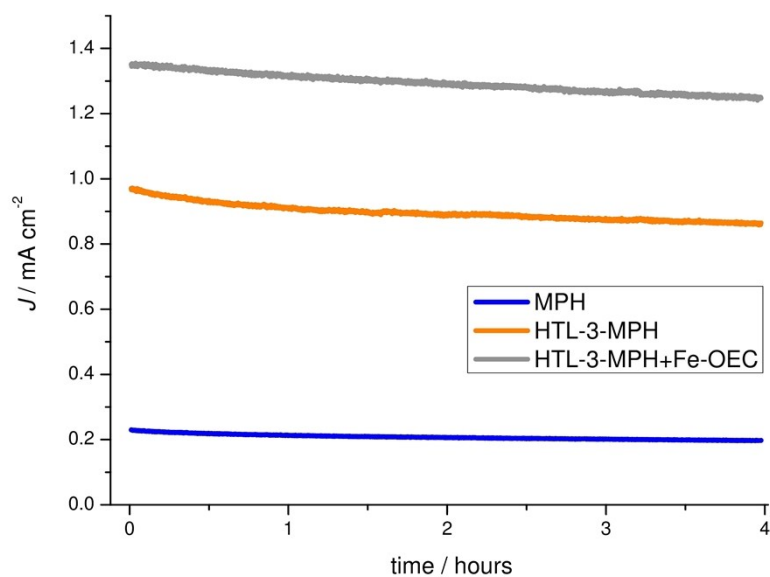


Figure S10 Chronoamperometry of MPH (blue line), HTL-3-MPH (orange line) and HTL-3-MPH+Fe-OEC (grey line) recorded in NaOH 0.1 M (pH 13.3) under continuous AM 1.5G illumination (100 mW cm^{-2}) at 0.6 V vs SCE.

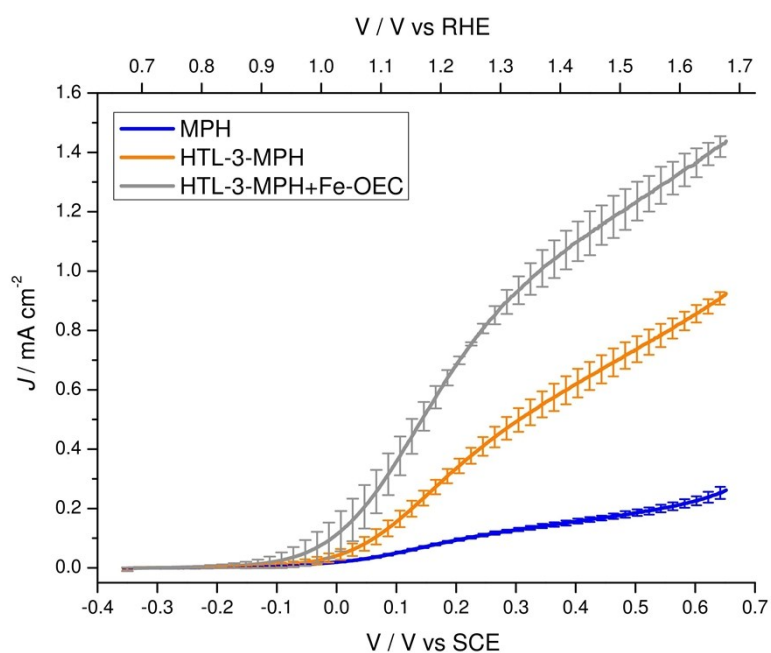


Figure S11 Average J - V response with their relative error bars of MPH (blue line), HTL-3-MPH (orange line) and HTL-3-MPH+Fe-OEC (grey line). The J - V curves reported are mediated over 12 different electrodes and measured in NaOH 0.1 M (pH 13.3) under AM 1.5G illumination (100 mW cm^{-2}).

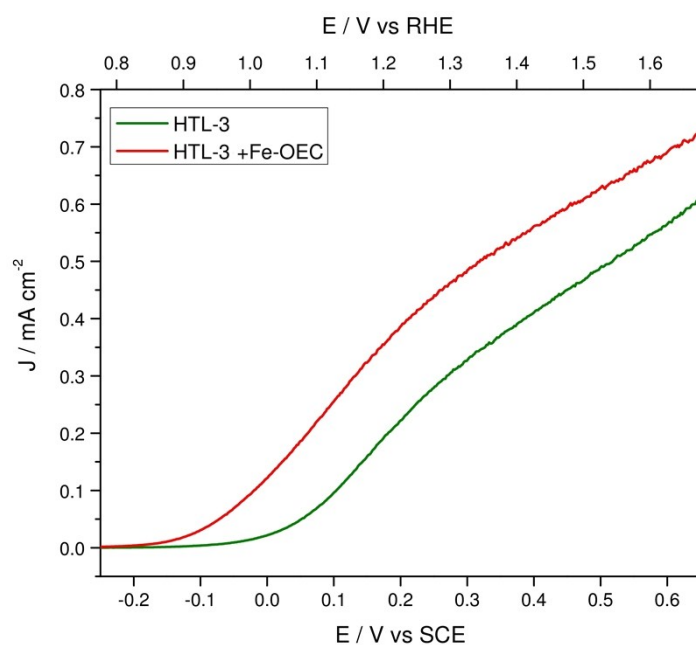


Figure S12 J - V curves under continuous illumination (100 mW cm^{-2} , AM 1.5G) of HTL-3 sample before (green line) and after (red line) functionalization with Fe-OEC recorded in NaOH 0.1 M (pH 13.3).

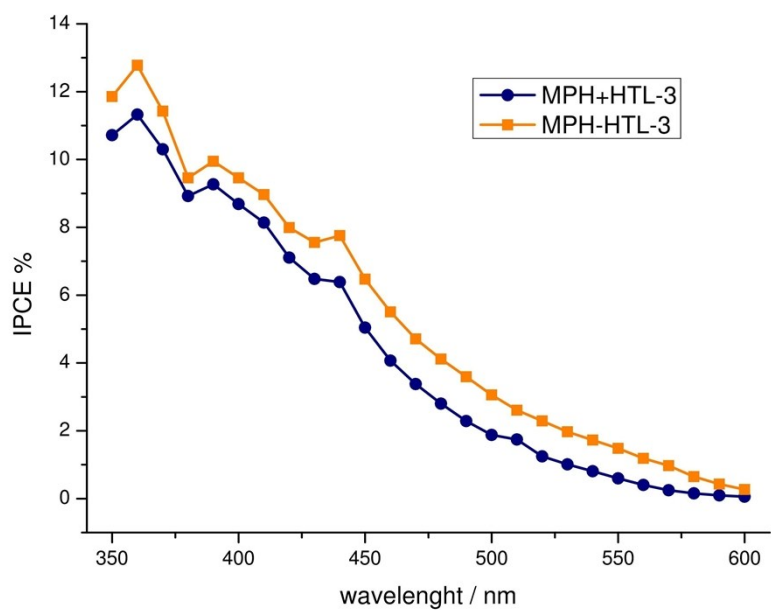


Figure S13 IPCE spectra of HTL-3-MPH (orange squares) compared to the summed individual contribution of MPH and HTL-3 (navy circles) FTO side illumination at 0.6 V vs SCE in NaOH (0.1 M, pH 13.3).

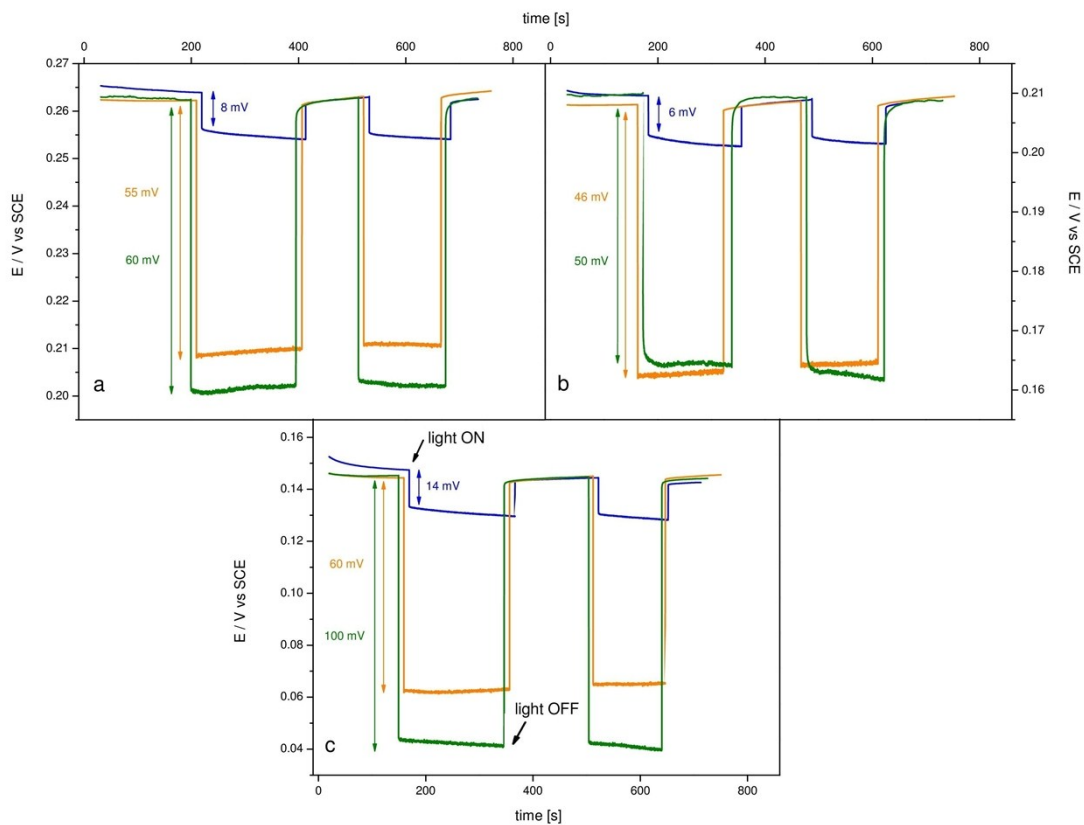


Figure S14 Photovoltage decays of MPH (blue line), HTL-3 (green line) and HTL-3-MPH (orange line) samples recorded at open circuit condition under shuttered illumination (100 mW cm⁻², AM 1.5G) in a KOH solution (0.1 M, pH 13.4) of K₄[Fe(CN)₆]/K₃[Fe(CN)₆] at three different concentrations: (a) 20 mM Fe(II)/200 mM Fe(III); (b) 100 mM Fe(II)/100 mM Fe(III); (c) 200 mM Fe(II)/20 mM Fe(III).

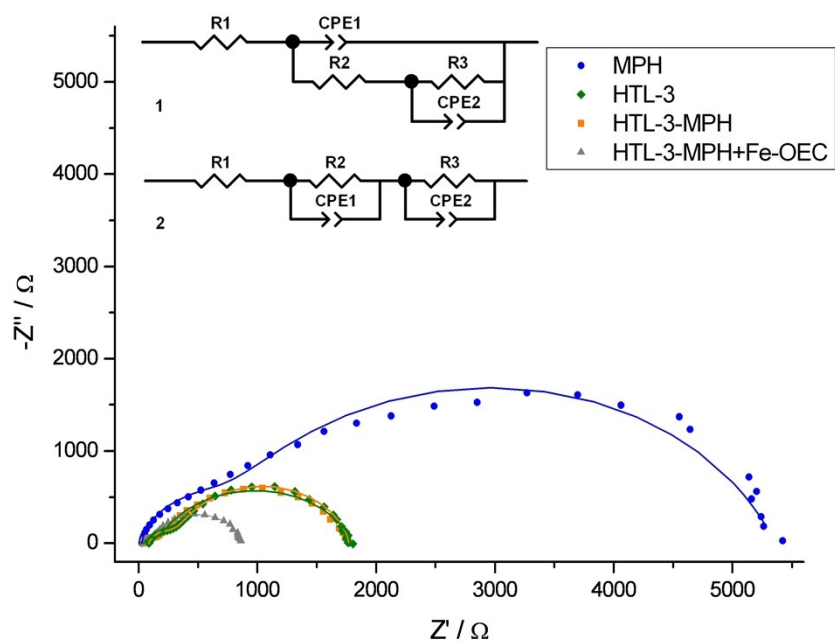


Figure S15 Nyquist plot (0 V vs SCE) of MPH (blue circles), HTL-3 (green diamonds) and HTL-3-MPH with (grey triangles) and without Fe-OEC (orange squares) recorded under AM 1.5G illumination (100 mW cm^{-2}) in NaOH (0.1 M, pH 13.3). Equivalent circuits used for fitting EIS data of (1) HTL-3 and HTL-3-MPH with and without Fe-OEC and (2) MPH electrodes are reported.

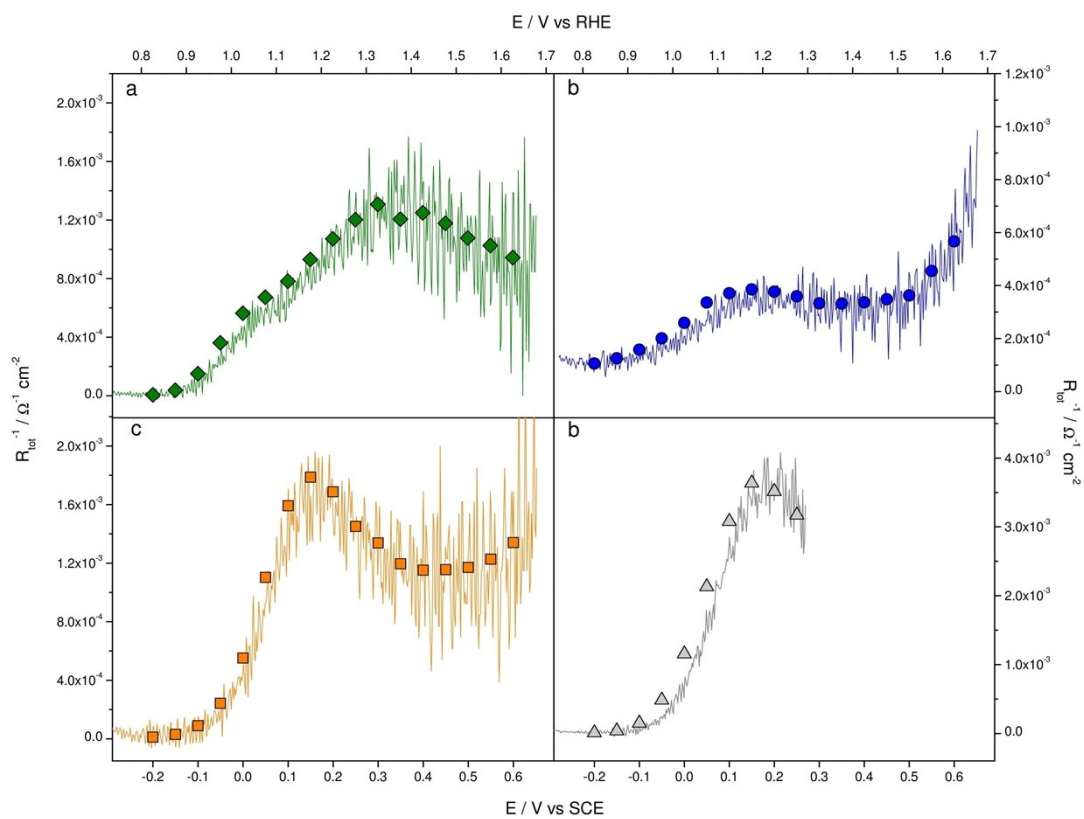


Figure S16 Derivative of the J - V curve (lines) compared to R_{tot}^{-1} obtained from EIS data (triangles) with models reported in Figure S14 for (a) HTL-3, (b) MPH, (c) HTL-3-MPH and (d) HTL-3-MPH with Fe-OEC samples.

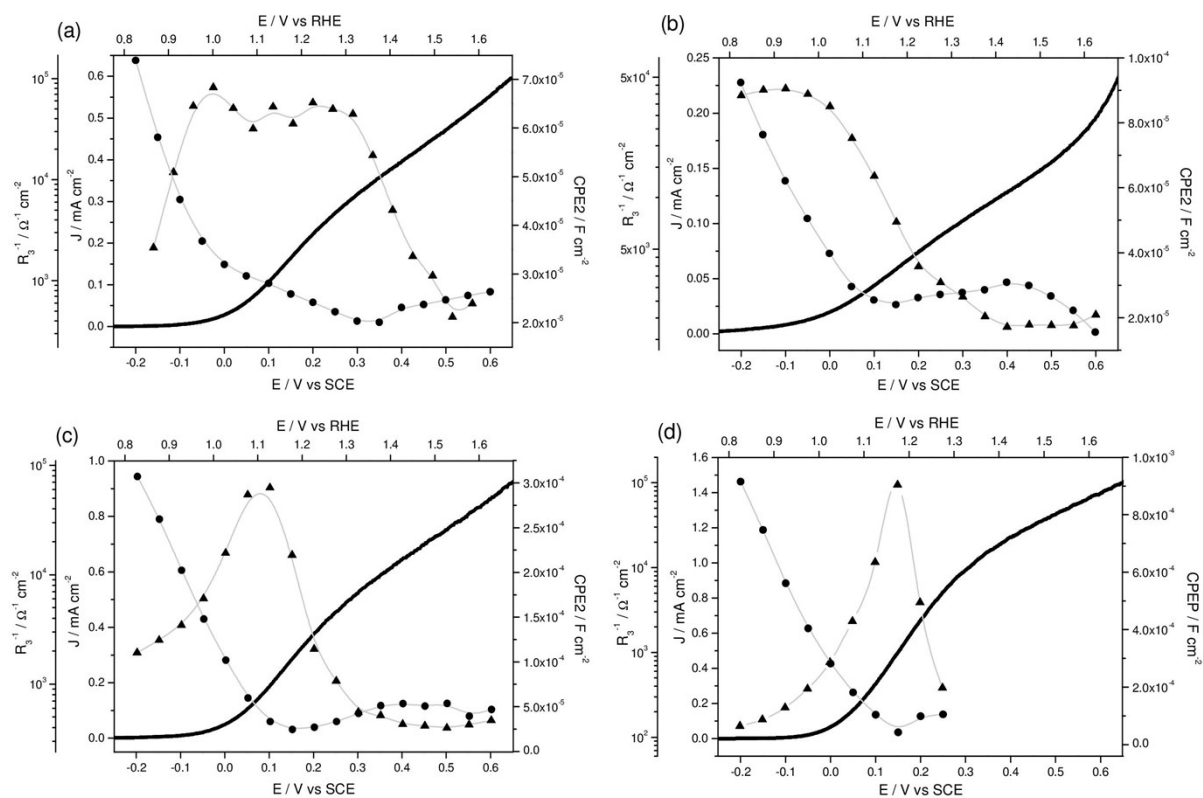


Figure S17 Plot reporting J - V curve (solid line), R_3 (circles) and CPE_2 (triangles) values obtained for (a) HTL-3, (b) MPH, (c) HTL-3-MPH and (d) HTL-3-MPH with Fe-OEC under AM 1.5 G illumination (100 mW cm^{-2}) in NaOH (0.1 M, pH 13.3).

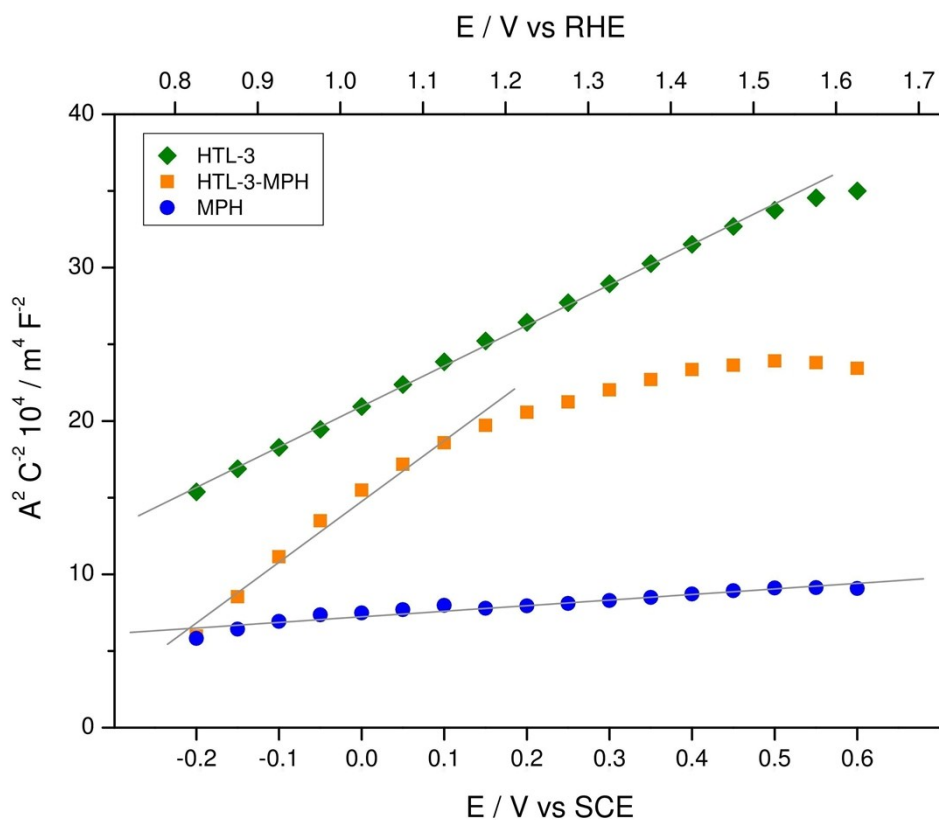


Figure S18 Mott-Schottky plot of MPH (blue circles), HTL-3 (green diamonds) and HTL-3-MPH (orange squares) recorded in the dark at 1 kHz in NaOH (0.1 M, pH 13.3). For MPH, the MS dependence is ascribed to FTO, whose roughness factor was considered the same as that of HTL (15), given that the latter is essentially conformal to the FTO, and $\epsilon = 10^1$ in the donor density calculations from MS fitting.

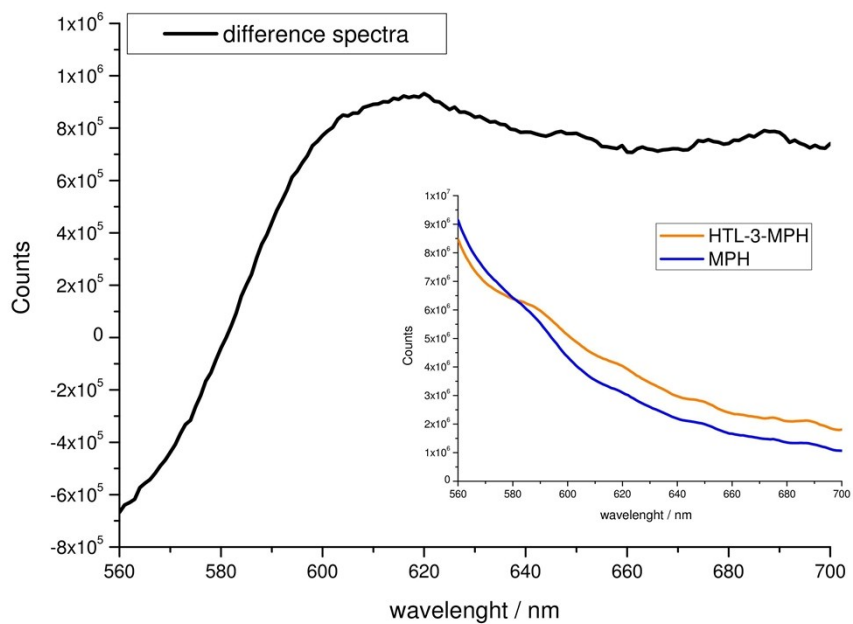


Figure S19 Difference photoluminescence emission spectra (PL) of HTL-3-MPH and MPH. (Inset) PL spectra (520 nm excitation light) of MPH (blue line) and HTL-3-MPH (orange line).

1. G. Boschloo and D. Fitzmaurice, *J. Phys. Chem. B*, 1999, **103**, 3093.